Development of sulfonated graphene oxide polyamide thin-film composite membranes for forward osmosis

Yeshan R. Galagedara[a,b], M. Gimhani N. Perera[a,b], Yiwei Ren[a,b,*], Mahesh Jayaweera[c], Yuntao Zhao[a,b], Rohan Weerasooriya[d]

[a]*Chongqing Institute of Green and Intelligent Technology, Chinese Academy of Sciences, Chongqing 400714, China,*
Tel. +8613666001586; email: renyiwei@cigit.ac.cn (Y. Ren), Tel. +8613220341454;
email: yeshan_galagedara@cigit.ac.cn (Y.R. Galagedara), Tel. +8613243524343;
email: gimhani_perera@cigit.ac.cn (M.G.N. Perera), Tel. +8615699933589; email: zhaoyuntao@cigit.ac.cn (Y. Zhao)
[b]*University of Chinese Academy of Sciences, Beijing 100049, China*
[c]*Department of Civil Engineering, University of Moratuwa, Katubedda, Sri Lanka, Tel. +94777320590;*
email: maheshjayaweera@gmail.com
[d]*Environmental Science Program, National Institute of Fundamental Studies, Hantana Road, Kandy, Sri Lanka,*
Tel. +94727172525; email: rohan@uwu.ac.lk

ABSTRACT

We fabricated a novel thin-film composite (TFC) membrane by integrating sulfonated graphene oxides (SGO) in its active layer. This novel membrane holds a great promise in forward osmosis (FO). The SGO was effectively synthesized from graphene oxide (GO), as it possesses a high hydrophilic nature, which in turn imparts enhanced desalination capacity for TFC-FO membranes. The structure and properties of TFC, GO-incorporated TFC membranes (GTFC) and SGO-incorporated TFC membranes (STFC) were characterized by attenuated total reflectance Fourier transform infrared spectroscopy (ATR-FTIR), scanning electron microscopy (SEM), and atomic force microscopy (AFM), and SGO incorporation was proven to be successful. Osmotic performance tests showed that STFC-FO membranes achieved higher water flux and reverse salt flux selectivity than GTFC-FO and TFC-FO membranes. The best STFC-FO membrane exhibited the water flux of 27.14 LMH with the specific reverse salt flux of 0.13 g/L. The SGO incorporation onto membrane also contributed to its decreased fouling propensity.

Keywords: Antifouling; Interfacial polymerization; Permeability; Reverse salt flux; Water flux

1. Introduction

Forward osmosis (FO) utilizes the osmotic pressure difference between feed and draw solutions to drive water across a semipermeable membrane with the rejection of other solutes [1–3]. FO-based technology is used in various applications, including desalination [4], wastewater treatment [5], membrane bioreactors [6], osmotic power generation [7], and food processing [8], etc. Compared with conventional pressure-driven membrane technology, FO has the advantages of low energy consumption, minimal fouling propensity, and high water recoverability [9,10].

Selection of an effective and efficient thin-film composite (TFC) is the key for the success of commercialized FO technology. Various types of FO membranes are available, among which polyamide (PA) TFC membrane has gained popularity because of its pH stability, high osmotic flux, and easy fabrication [11,12]. Utilizing interfacial polymerization (IP), TFC-FO membranes are often fabricated by depositing an ultra-thin active

* Corresponding author.

PA layer on a substrate material (i.e., support layer) [13]. To date, much attention is paid to optimize the chemical and structural properties of the support layer [14,15]. Although less attention is paid to modifications of the active layer, it plays a vital role in determining the osmotic performance of TFC-FO membrane [16]. Recently, nanostructured materials, such as zeolite, TiO_2, carbon nanotubes, and graphene oxide (GO) have been incorporated into PA layers [17–19]. Interestingly, the water flux and salt rejection for such nanocomposite membranes with optimum nanomaterial loadings have been greatly improved. GO, a novel two-dimensional carbon sheet acquires attraction in developing high-performance thin-film nanocomposite membrane for water treatment and desalination due to its abundant hydrophilic oxygen-containing functional groups (e.g., carboxyl, epoxy, and hydroxyl). It has been revealed that GO-embedded PA reverse osmosis (RO) and FO membranes show superior permselectivity, chemical robustness, and anti-fouling capacity [20,21].

This paper addresses the possibility of incorporation of sulfonated graphene oxide (SGO) instead of GO for further improvement of the performances of FO membranes. Moreover, GO nanosheets possess unique graphitized planar structures, which facilitate further surface functionalization to increase its hydrophilicity by substituting hydroxyl/epoxy groups with the sulfanilic group without damaging morphology [22]. It has been reported that the pure water permeability of SGO-embedded polyvinylidenefluoride ultrafiltration membrane was higher when compared with that of the GO-incorporated membrane [23]. So far to our knowledge, there has been no work available on SGO-embedded PA-TFC FO membranes.

In this work, the GO surface sites were successfully functionalized with sulfonic acid groups. The synthesized SGO was integrated into the PA-TFC FO membrane via in situ IP of M-phenylenediamine (MPD)-SGO and trimesoyl chloride on a porous substrate. Effects of SGO loadings on the physiochemical properties, osmotic performance, and antifouling of FO membrane were investigated systematically.

2. Materials and methods

2.1. Materials

GO (average diameter 0.5–5.0 μm, average thickness 0.6–1.0 nm, 99.95% purity) was purchased from Hengqiu Graphite Co., Ltd., Suzhou, China. Polysulfone (PSF) beads, dimethylacetamide (DMAc), sodium nitrate ($NaNO_3$, 99%), n-hexane (97%, anhydrous), sodium chloride (NaCl, 99.5%), sodium alginate (SA, Mwt.: 98.11), potassium dihydrogen phosphate (KH_2PO_4, 99.5%), magnesium sulfate ($MgSO_4$, 99%), sodium bicarbonate ($NaHCO_3$, 99.5%), calcium chloride ($CaCl_2$, 96%), and ammonium chloride (NH_4Cl, 99.5%) were procured from Kelong Co., Ltd., Chengdu, China. The MPD (99.5%) and 1,3,5-benzene-tricarbonyl trichloride (TMC, 98%) were stored in a refrigerator before being used.

2.2. SGO synthesis

The SGO synthesis was carried out in several steps. Firstly, the diazonium salt of sulfanilic acid was prepared by mixing 0.5 g of sulfanilic acid with 2% NaOH in a sonicator (EBT Series Ultrasonicator, China) to yield maximum dispersal; subsequently, $NaNO_3$ and concentrate HCl were added to the sonicated mixture with continuous stirring. To synthesize SGO, diazonium salt of the sulfanilic acid and 2 g/mL GO suspensions were mixed in an ice bath under vigorous shaking for a 3-h period. SGO particulates were then separated by centrifugation at 6,000 rpm. After drying for 8 h, SGO was collected in powder form [24].

2.3. Fabrication of membrane substrates

As detailed elsewhere [25], membrane substrates were fabricated by the non-solvent induced phase separation method. Briefly, 15% (wt.) PSF polymer beads were dissolved in 85% (wt.) DMAc solution under constant stirring at ambient conditions for 1 d; after that, the solution was stored overnight in a desiccator to eliminate air bubbles. The polymer solution thus prepared was cast onto a pre-cleaned glass plate and then immersed in a deionized (DI) water bath at room temperature for 10 min to facilitate phase separation. The DI water was changed every 12-h period of 2 d to minimize the residual solvents being deposited on the membrane. Subsequently, the membrane substrate was stored at 5°C until further use.

2.4. Deposition of PA active layer

GO-incorporated thin-film PA layer was laid on membranes via in situ IP. A series of GO/MPD solutions (GO concentration between 0–800 ppm [0, 100, 200, 400, and 800 ppm] in 2% (wt.) MPD) were prepared. GO particulates were well dispersed in the MPD solution with sonication for a 3-h period. Similarly, a series of SGO/MPD solutions were prepared. The IP method was used to embed GO/MPD and SGO/MPD onto the membrane surface. After cleaning with DI water, membrane substrates were immersed in GO/MPD and SGO/MPD solutions to yield GO- and SGO-MPD saturated membranes. After removing excess MPD from membrane surfaces, 1% (w/v) TMC/hexane solution was poured onto the membrane substrates to facilitate induced-polymerization, and be drained off after 1 min. The resulting GO- and SGO-embedded membranes were first dried in the air and then in an oven at 60°C for a 2-min period. Finally, they were stored in DI water at 5°C until further use. No nanomaterial-embedded, GO-, and SGO-TFC membranes were designated as TFC, GTFC-1, GTFC-2, GTFC-4, GTFC-8, STFC-1, STFC-2, STFC-4, and STFC-8 (TFC: TFC with no nanomaterial-embedded; GTFC-1: GO-embedded thin-film membranes with 100 ppm of GO, and STFC-1: SGO-embedded thin-film membranes with 100 ppm of SGO), respectively.

2.5. Characterization of GO, SGO, TFC, GTFC, and STFC membranes

GO and SGO were characterized by FTIR (Cary 630, Agilent, USA) and X-ray diffraction (XRD) (D8 Advance-2, Bruker, USA) to ensure that nanosheets were successfully formed. Field emission electron microscopy (FE-SEM, JSM-7800F, Jeol, Japan) was used to examine the surface morphology of all fabricated membranes. The samples were vacuum dried at room temperature for a 24-h period. The interactions of GO and SGO with substrates were studied using freeze-dried membrane

surfaces and cross sections, which were fractured in liquid nitrogen to protect the pore structures. All samples were gold-coated by sputtering (SCD 050, BAL-TEC, Germany). Contact angle measurements were made with the applied sessile drop method. Leveled membrane surfaces interacted with tiny droplets of DI water (5–7 μL), and the images were taken for side elevations of water droplets; contact angles were determined by an image processing software using five points' averaging. The surface roughness of the membranes was determined by atomic force microscopy (TT2 AFM, AFM Workshop, USA). In roughness determination, the vacuum-dried membranes and the strips were kept on a cover glass for AFM observations. Data were collected from several points to calculate the mean roughness. The functional groups in TFC as identified by FTIR and the absorbance of the amide (1,660 cm^{-1}) and PSF (1,323 cm^{-1}) groups were used to determine the membrane thickness [26].

2.6. Determination of water flux, permeability, and salt rejection

Regarding water flux (J_v), reverse salt flux (J_s), and specific reverse salt flux (J_s/J_v), the osmosis performance of the as-prepared TFC-FO membranes were obtained through a custom cross-flow FO system as presented in our previous work [27]. During tests, feed solution (FS) and drive solution (DS) were pumped concurrently at a velocity of 6.4 cm/s along membrane surface. All the tests were performed under both FO mode (FS against active layer) and pressure-retarded osmosis (PRO) mode (DS against active layer) with DI water taken as the FS. In FO mode, NaCl solutions of four concentrations (0.5, 1, 1.5, and 2 M) were prepared and used as DS. In PRO mode, 1.0 M NaCl solution was applied as DS. The changes in conductivity of FS and weight of the DS were recorded automatically through a conductivity meter (DDSJ-308A, INESA Scientific Instrument, China) and digital balance (BSA6202S-CW, Sartorius, Germany), respectively. Each test was conducted for about 30 min and was repeated three times with different membrane sections. The J_v (Lm^{-2}h^{-1} or referred to as LMH) was calculated by Eq. (1):

$$J_v = \frac{\Delta V}{A_m \times \Delta t} \tag{1}$$

where ΔV (L) is the permeate water volume over a period Δt (h), and A_m (m^2) represents the test area of the membrane. The water density is calculated to be 1,000 g/L. The J_s (g m^{-2} h^{-1} or referred to as gMH) was calculated by Eq. (2):

$$J_s = \frac{C_t V_t}{A_m \Delta t} \tag{2}$$

where C_t (g/L) and V_t (L) are the draw solute (NaCl) concentration and volume of FS over time Δt, respectively. The C_t was estimated based on a standard curve of draw solute concentration as the conductivity.

2.7. Determination of membrane properties

The intrinsic properties (water permeability [A], and salt permeability [B]) of the TFC-FO membranes were estimated by following the standard testing procedure introduced by Tiraferri et al. [28].

2.8. Antifouling test

1.5-L two synthetic wastewater solutions composed of compositions of solution 1 with 0.45 mM KH$_2$PO$_4$, 9.20 mM NaCl, 0.61 mM MgSO$_4$, 0.5 mM NaHCO$_3$, 0.5 mM CaCl$_2$, and 0.93 mM NH$_4$Cl in DI water and Solution 2 with the same compositions as of Solution 1 together with 250-mg/L SA as organic foulant were prepared. During the cleaning route, the FS (DI water) and DS (1 M NaCl) solutions were circulated at a rate of 0.3 Lmin^{-1} (150 rpm) by gear pumps. Solution 1 was used as FS, and 2 M NaCl was used as DS for 1-h operation period to stabilize water flux (J_v). In the second step, FS was changed into Solution 2 while 2 M NaCl was used as DS for an 18-h period. Physical cleaning of the membrane was carried out using 2 M NaCl for both FS and DS at 300 rpm (0.6 Lmin^{-1}) for a 30-min period. During the third step, FS was switched to DI water, and DS remained as 2 M NaCl for a 30-min period of operation.

The flux reduction ratio and flux recovery ratio (FRR%) were calculated by Eqs. (3) and (4) to determine the antifouling propensity:

$$FR\% = \frac{J_o - J_t}{J_o} \times 100\% \tag{3}$$

$$FRR\% = \frac{J_c}{J_o} \times 100\% \tag{4}$$

where J_o is the initial flux; J_t is the flux after accelerated fouling test, and J_c is final water flux after the physical cleaning stage.

3. Results and discussion

3.1. Characterization of GO and SGO nanoparticles

The results of FTIR analyses (Fig. 1) depicted the differences between the GO and SGO by absorbance spectra. The presence of functional groups of C=O bonds (1,618 cm^{-1}),
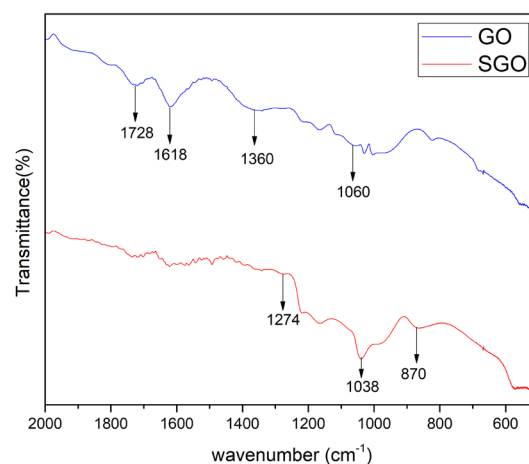

Fig. 1. FTIR spectra of GO and SGO.

C–OH (1,360 cm^{-1}), and C–O (1,060 cm^{-1}) was observed in the FTIR spectrum of GO confirming carboxyl, hydroxyl, and epoxy groups, which was also analogous to work reported elsewhere [15]. The appearance of characteristic peaks at 1,274, 1,038, and 870 cm^{-1} corresponds, respectively, to the presence of the asymmetric stretching of O=S=O, stretching of S=O, and S–O functional group in the sulfonic acid group in SGO, confirming that the sulfonic acid group was attached to GO surface successfully [23]. The spectrum of SGO, therefore, indicated the successful functionalization and surface modification of GO by diazonium salt. The peaks corresponding to 1,728, 1,618, 1,360, and 1,060 cm^{-1} in the SGO spectrum were attributed to partial reduction because of the replacement of the carboxyl, hydroxyl, and epoxy functional groups with the sulfanilic group.

To further demonstrate the effective synthesis of SGO, it was characterized by XRD. The XRD spectra of GO and SGO are shown in Fig. 2. The sharp peak at 2θ=9.10° indicated the reflection of GO [20]. In SGO at 2θ=18.05°, there was a significant correlation with the sulfanilic group [29]. This phenomenon suggested that GO was transformed into SGO with relevant functional groups successfully.

3.2. Characterization of GO- and SGO-embedded TFC-FO membranes

Incorporating hydrophilic nanomaterials into the membrane-active layer is capable of improving the performance of resultant TFC-FO membranes. The FTIR spectra of the TFC, GTFC, and STFC membrane series (not shown) manifested almost similar patterns. The peaks corresponding to the functional groups of GO and SGO were not readily observed due to the minute amounts of nanomaterial loadings and the near-overlapping effect. However, the characteristic peaks were observed at 1,660 and 1,543 cm^{-1} in both spectra due to the formation of PA groups by IP, associated with Amide I (carbonyl stretching vibration) and Amide II (C–N stretching and coupling of the in-plane N−H bending vibration), respectively [30]. Further, the PA layer thickness of GTFC and STFC membrane series was determined by FTIR data. As shown in Fig. 3, the ratio of
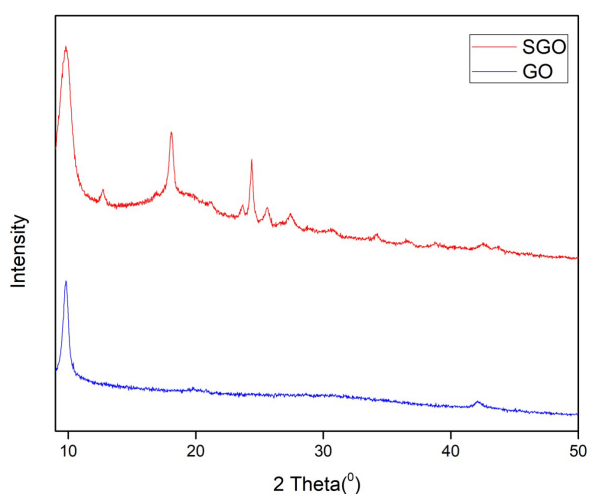
absorption peak intensity of the amide (–CONH–) to sulfone (–SO$_2$–) groups was expressed as a quantitative implication for its PA layer thickness [26]. It can be seen in Fig. 3 that when the GO and SGO loading increased, the thickness of skin-layer first decreased to reach a minimum and then increased with the overloading of nanomaterials. A thinner PA layer with a low-intensity ratio may result in the reduction of mass transfer resistance seriously, which then leads to the improved water flux [31].

Fig. 4 illustrates the top surface morphologies of TFC, GTFC-4, and STFC-4 membranes. As a result of the interaction between MPD and TMC during the IP process, a uniform top-surface was pronounced clearly in each membrane sample. The images appeared in such a way that all the modified membranes possessed a typical morphological characteristic called "ridge-and-valley morphology" [32]. The SEM images of the top surfaces manifested, that there were two distinctly different structures; namely, leaf-like and nodular-like structures. Nevertheless, there were no distinctly different changes in SEM images.

Fig. 4 also displays three-dimensional AFM images of TFC, GTFC-4, and STFC-4 membranes. The mean roughness of the membrane surfaces was estimated from AFM data and presented in Fig. 5 for all membranes. Both GTFC and STFC membranes showed smooth surfaces with low surface roughness. Such a phenomenon leads to higher water solubility, which stimulates the water uptake rate during the IP [33,34]. The formation of smooth surfaces with low surface roughness corresponds to the optimum reaction mechanism during the IP, and it could be because of the active groups of GO and SGO reacting with the MPD and TMC, giving rise to a higher reaction rate in the IP process. Moreover, hydrogen bonds present in the sulfanilic group of SGO and the hydroxyl group of GO could warrant a more compact chain structure. According to the Langmuir–Blodgett film deposition theory, deposition of nanosheets usually changes in horizontal alignment, impeding the diffusion of MPD into the organic phase, so that it produces prominent smooth surfaces [35]. However, when excess solutes on the GO and SGO are
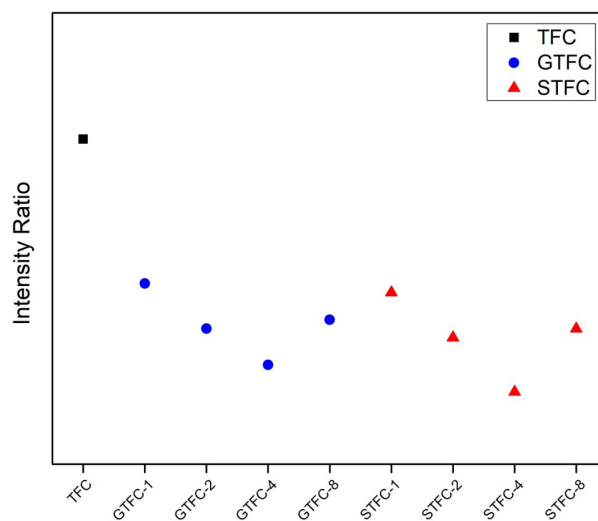

Fig. 2. X-ray diffraction patterns of the GO and SGO.

Fig. 3. Ratio of absorption peak intensity of amide (–CONH–) to sulfone (–SO$_2$–) groups of TFC, GTFC, and STFC membranes.
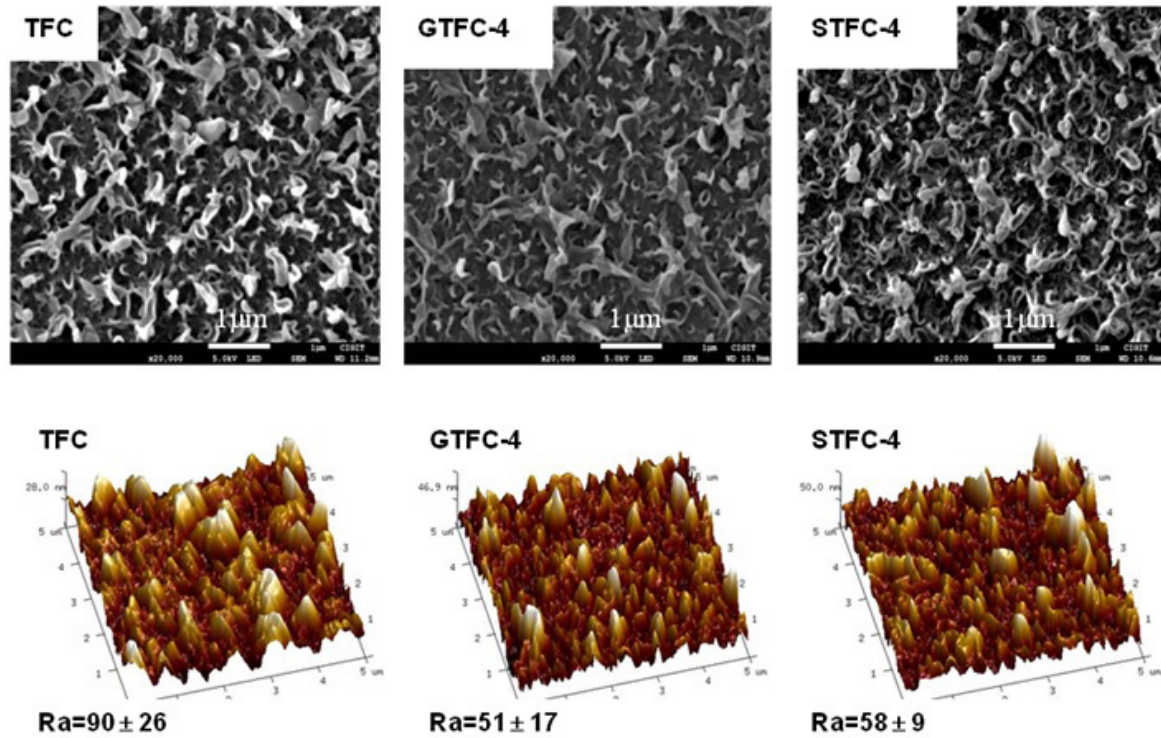
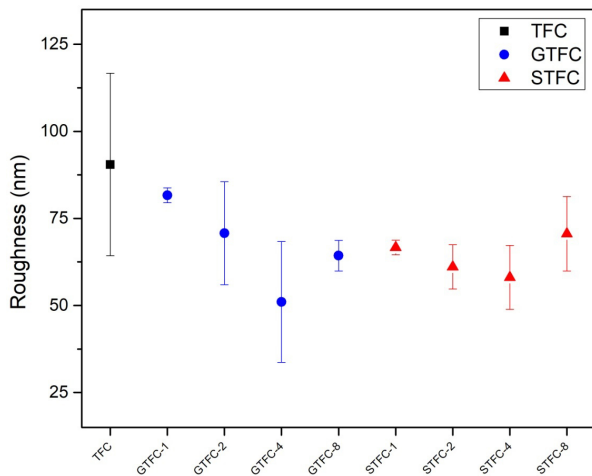Fig. 4. SEM and AFM images of surface morphologies in TFC, GTFC-4, and STFC-4 membranes.

Fig. 5. Variations of surface roughness of TFC, GO, and SGO membranes.

Table 1
Intrinsic transport properties of TFC, GTFC, and STFC membranes

Membrane ID	A, LMHbar^{-1}	B, LMH	B/A, bar
TFC	1.23 ± 0.08	0.73 ± 0.03	0.59
GTFC-1	1.86 ± 0.07	0.68 ± 0.02	0.37
GTFC-2	2.59 ± 0.03	0.65 ± 0.02	0.25
GTFC-4	3.19 ± 0.02	0.61 ± 0.01	0.19
GTFC-8	2.19 ± 0.04	0.65 ± 0.03	0.30
STFC-1	2.81 ± 0.06	0.61 ± 0.04	0.22
STFC-2	3.57 ± 0.05	0.55 ± 0.03	0.15
STFC-4	4.10 ± 0.04	0.52 ± 0.04	0.13
STFC-8	3.16 ± 0.07	0.59 ± 0.03	0.19

present, they tend to agglomerate in the interfacial region affecting the structural integrity of the top surface while reducing the water permeation flux [36].

3.3. Intrinsic separation performance

The intrinsic transport properties, including water permeability coefficient (A) and salt permeability coefficient (B) for different GO- and SGO-modified TFC membranes are presented in Table 1. As mentioned above, nanomaterial loading in active layer could influence the properties of the membranes and hence, alters the transport properties. It can be observed that the water permeability (A) values were higher in STFC membrane series when compared to those of GTFC series. While the water permeability being the highest, the lowest salt permeability was recorded in STFC membrane series compared with that of the TFC and the corresponding GTFC membranes. In comparison, STFC-4 was found to have the highest A value (4.10 ± 0.04 LMH bar^{-1}) and the lowest B value (0.52 ± 0.04 LMH), which provides superior membrane performances. As shown in the data, the intrinsic selectivity (B/A) factor was the lowest in STFC-4 (0.13 bar). The incorporation of GO and SGO leads to enhance the passage of water via the interfacial gap between nanosheets and PA. The overall water permeability through the STFC membrane depends on two factors; membrane hydrophilicity enhancement by –SO$_3$H, –COOH, and –OH groups capable of attracting water molecules, which facilitate their passage

effectively and reduction of membrane PA layer thickness that is attributed to low transport resistance [36]. Therefore, it is evident that the formation of a thin skin layer due to the presence of nanosheets plays a major role toward membrane hydrophilicity.

The observed trends in water permeability of GO- and SGO-assimilated TFC membranes were elucidated in terms of the water contact angle. As shown in Fig. 6, it was in agreement with published data [15,18,20,23], that the water contact angle of TFC membrane was about 85.86°, but was reduced sharply as low as 56.00° with SGO loading up to 400 ppm. The abundance of oxygen-rich functional groups such as –OH, –COOH, and –SO$_3$H in SGO enhanced the hydrophilicity reducing the contact angle values. Although not conclusive, the increased contact angles in GTFC and STFC membrane series may be ascribed to interwoven hydrogen bonding [37]. Membranes with higher values of hydrophilicity represented by the presence of active/functional groups can form hydrogen bonds with the aqueous solution in contact. Moreover, greater charge density on the membrane surface due to –SO$_3$H group warrants greater membrane hydrophilicity. However, further increase in SGO loading to 800 ppm slightly increased the contact angle to 66.43° resulting in lower water permeability. It was also noted that permeability trends of pure water could not solely be accounted for the contact angle measurements. Our results justified that the SGO-incorporated TFC membranes yield greater water permeability when compared with the controlled and GO-incorporated membranes and exhibit excellent FO performance.

3.4. Determination of osmosis flux performance of TFC-FO membranes

The TFC and nanomaterial-integrated TFC membranes were further investigated under FO and PRO modes using DI water as the FS and 1 M NaCl as the DS. Figs. 7–9 depict the osmotic water flux (J_w), reverse salt flux (J_s), and specific salt flux (J_s/J_w) for GO- and SGO-incorporated TFC membranes, respectively. The GO- and SGO-assimilated membranes showed substantial differences in performance compared to the TFC membrane. In the controlled TFC membrane, water flux was estimated to be 14.26 LMH, and the same for the SGO-embedded membranes was higher (27.14 LMH)
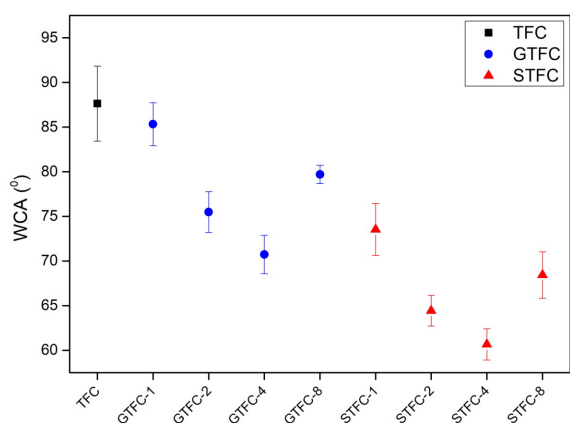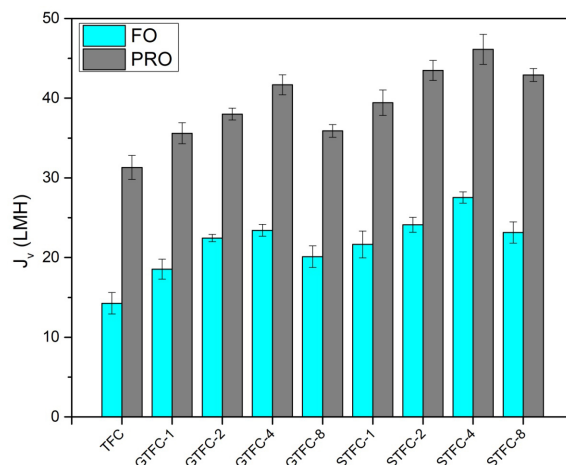

Fig. 7. Water flux of TFC, GO-, and SGO-incorporated TFC membranes.
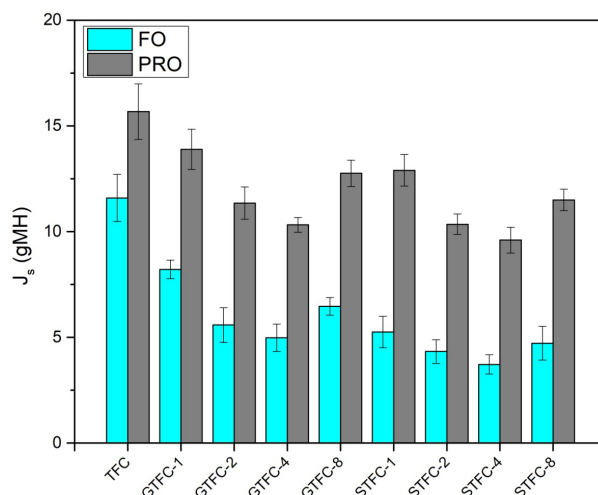

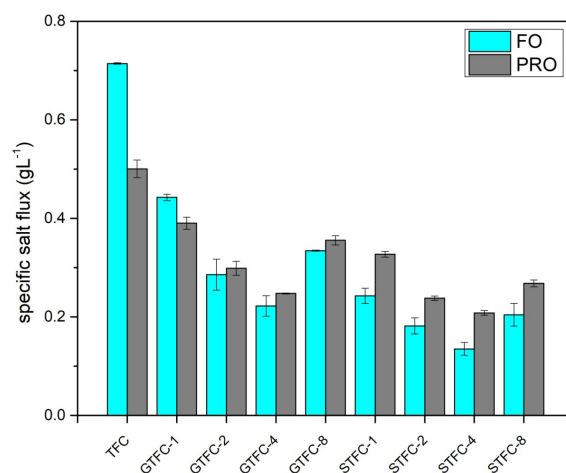Fig. 8. Reverse salt flux of TFC, GO-, and SGO-incorporated TFC membranes.

Fig. 9. Specific salt flux of TFC, GO-, and SGO-incorporated TFC membranes.

Fig. 6. Water contact angles of TFC, GTFC, and STFC membranes.

revealing 90% increment in osmotic water flux compared with that of the controlled TFC membrane while the same for GO-assimilated ones was 23.14 LMH giving an increase of 62%. This observation could have been due to the reduced thickness of the STFC membranes compared with other membranes. However, water flux in the PRO mode was higher than that in the FO mode for all membranes demonstrating that the internal concentration polarization in the FO mode was more severe than that in the PRO mode. Moreover, the water flux of the GTFC membranes was also improved due to its oxygen-loving, functional groups (–COOH/–OH), which attract water molecules and facilitate their transport through the membrane. Further, the addition of SGO greatly influenced the enhancement of water flux [38], reaching the peak value of 27.14 LMH for STFC-4 membrane. This observation revealed that the presence of sulfanilic groups (–SO$_3$H) was capable of accommodating a thinner water hydrogen layer and stronger hydrogen bonding resulting in an escalation of the water flux [22]. Moreover, this escalation in water flux was attributed to the combined effect of the enhanced hydrophilicity, thinner selective layer, and additional passages formed. In contrast, the improvement of water flux was slightly decreased in the high content of SGO (800 ppm) mainly on account of agglomerated SGO nanoparticles acting as a barrier to the water passage [15,35]. When relatively low SGO loadings (100, 200, and 400 ppm) were performed, the hydrophilicity could be the major factor for higher water flux whereas it became a hindrance to enhanced water flux with higher loadings of SGO (800 ppm). The overall water flux performance of the SGO-embedded membranes was remarkably increased as a result of high membrane surface roughness, low contact angle and low thickness.

Fig. 8 indicates the reverse salt flux as a function of GO or SGO concentration. Initially, the reverse salt flux decreased sharply until SGO loading reached 400 ppm and then increased for the loading of 800 ppm, which is analogous to the similar pattern obtained for water flux. In the case of a solute diffusion, the solute flux is inversely proportional to the salt rejection coefficient [2], which emphasizes that low solute flux is attributed to higher salt rejections, which is a desirable condition for FO membranes. The specific salt flux, Js/Jw of the STFC membrane with 400 ppm of SGO was reported to be 0.136 g/L, indicating that this membrane possesses the lowest specific salt flux. Hence, when considering factors such as water flux, contact angle, water permeability, and salt permeability, it is inferred that 400 ppm of SGO could diligently be used as the optimum dosage to be incorporated into the TFC membrane.

3.5. Anti-fouling

Membrane fouling is an inevitable phenomenon in FO process, which can be detected by cyclic filtration tests and was studied with the controlled TFC, GO-, and SGO-incorporated membranes under FO mode (Fig. 10). Experiments were carried out with the presence of SA as a foulant containing calcium ions to evaluate the behavior of foulant on the membrane active layer. During the membrane filtration process, the water flux of the SGO-incorporated TFC membrane was relatively lower than that of the GO-incorporated membrane as illustrated in Fig. 8.

Our results indicated the reduction of DS concentration was due to the addition of a foulant at the initial stage. However, the addition of SA influenced all membranes by reducing water flux considerably due to firm attachment and adsorption of protein molecules on the membrane surface or membrane pores [38,39]. This phenomenon eventually clogs the water-passing channels, which subsequently results in a decline of water flux. On the other hand, the formation of cross-linked alginate gel layer would attach to calcium ions, which acts as a bridge between alginate molecules and calcium ions [40,41]. After membrane cleaning, the pure water flux of all membranes could not be entirely reinforced up to their initial levels. GO- and SGO-incorporated membranes manifested profoundly higher restoration rates compared with that of TFC membrane (Fig. 11). This scenario indicates the formation of a thinner SA gel layer on STFC due to surface properties of hydrophilicity and surface smoothness by incorporating sulfanilic group. When deposition of proteins on the membrane surface occurs loosely, it is
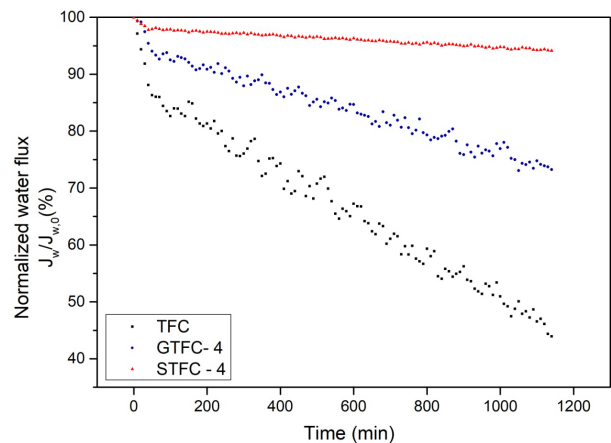

Fig. 10. Forward osmosis fouling test of TFC, GTFC, and STFC membranes (2M NaCl solution and synthetic wastewater were used as DS and FS, respectively; the $J_w/J_{w,o}$ ratio was taken with a 10-min interval during the fouling test).
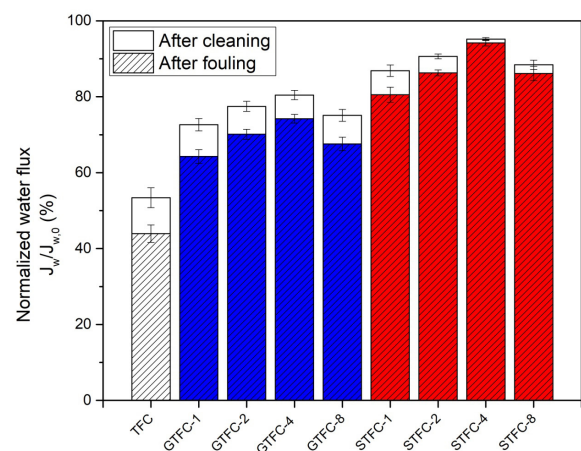

Fig. 11. Forward osmosis fouling test results of TFC, GO-, and SGO-incorporated TFC membranes (2M NaCl solution and synthetic wastewater were used as DS and FS, respectively).

recognized as reversible fouling and could be removed by hydraulic cleaning. On the other hand, direct attachment of protein molecules on the membrane surface and pores is recognized to be irreversible fouling, which seems difficult to be removed. This scenario implicates that the modified membranes undergo reversible fouling while TFC membrane is affected by irreversible fouling due to its hydrophobic interactions between the foulant and the membrane surface. Furthermore, the accumulation of hydrophilic –SO₃H groups in SGO-incorporated TFC membranes are capable of enhancing the density with a stable hydration layer when compared with that in –COOH groups with GO-incorporated TFC membrane. It is evident in Fig. 8 that the TFC membrane was composed of the minimum FRR of 53%, while the same of GTFC-4 and STFC-4 membranes was heightened to 81% and 95%, respectively.

Improved antifouling in SGO-embedded membranes could be associated with many aspects such as surface charge, surface tension, and electrostatic forces. Foulants are often negatively charged, and such negative charges on the membrane surface are increased, a strong electrostatic repulsion force could be generated, which will then lead to an enhanced antifouling performance. Accordingly, STFC membrane rich in functionalized sulfonic acid groups is more negatively charged than the GTFC with carboxyl, hydroxyl, and epoxy groups due to the existence of an additional oxygen atom in the sulfonic acid group, which will result in higher reversible fouling [42]. Another governing factor is the surface tension/interfacial free energy, which tends to be high for hydrophilic surfaces and low for hydrophobic surfaces. Therefore, the hydrophobic particles influence to cluster colloidal particles due to low interfacial free energy. Thus, fouling could be reduced by modifying membranes with more hydrophilic characteristics, which are attributed to sulfonic acid groups in the case of STFC membranes. Also, the protein adsorption onto membrane is affected by Van der Waals, hydrogen bonding, and electrostatic forces. Therefore, strongly bound water molecules could attach to the hydrophilic surface through hydrogen bonding hindering progressively the adsorption of foulants, which is influenced by increased hydrogen bonding force caused by ionized sulfonic acid groups on the STFC membrane surfaces with the removal of foulants as a loose cake layer. Meanwhile, the high electrostatic repulsion forces inhibit protein adsorption and also remove the attached foulants. According to the contact angle measurements carried out (Fig. 6), STFC membrane had more hydrophilicity, and as a result, SGO-embedded TFC membrane could stimulate high hydrophilicity and consequently, makes robust antifouling capabilities.

4. Conclusion

Novel SGO-incorporated TFC membranes were synthesized using the IP process, and the effects of the sulfanilic groups on the performance of modified membranes were investigated. The contact angle of the STFC membranes decreased, and the permeability improved simultaneously. The STFC-series membranes possessed smooth surfaces with low surface roughness. STFC-4 showed the highest water flux (33.87 LMH) compared with TFC membrane (20.65 LMH) and GTFC-4 membrane (31.56 LMH). The optimal membrane performance was reported in STFC-4 with a 95% FFR ratio. STFC-series membranes possess superior properties required for fabrication of TFC for FO technology.

Symbols

A	—	Water permeability
A_m	—	Effective membrane area
B	—	Salt permeability
C_f	—	Feed concentration
C_p	—	Permeate concentration
C_t	—	Salt concentration
DS	—	Draw solution
FO	—	Forward osmosis
FRR%	—	Flux recovery ratio
FS	—	Feed solution
GO	—	graphene oxide
GTFC	—	Graphene oxide-incorporated thin-film composite
J_c	—	Final water flux after the physical cleaning
J_o	—	Initial flux
J_s	—	Reverse salt flux
J_s/J_v	—	Specific salt flux
J_t	—	Flux after accelerated fouling test
J_v	—	Water flux
PA	—	Polyamide
PRO	—	Pressure-retarded osmosis
SGO	—	Sulfonated graphene oxide
STFC	—	Sulfonated graphene oxide-incorporated thin-film composite
TFC	—	Thin-film composite
Δt	—	Test time
ΔV	—	Volume change

References

[1] A. Subramani, J.G. Jacangelo, Emerging desalination technologies for water treatment: a critical review, Water Res., 75 (2015) 164–187.

[2] T.Y. Cath, A.E. Childress, M. Elimelech, Forward osmosis: principles, applications, and recent developments, J. Membr. Sci., 281 (2006) 70–87.

[3] N. Akther, A. Sodiq, A. Giwa, S. Daer, H.A. Arafat, S.W. Hasan, Recent advancements in forward osmosis desalination: a review, Chem. Eng. J., 281 (2015) 502–522.

[4] T. Chung, X. Li, R.C. Ong, Q. Ge, H. Wang, G. Han, Emerging forward osmosis (FO) technologies and challenges ahead for clean water and clean energy applications, Curr. Opin. Chem. Eng. J., (2012) 246–257.

[5] R.W. Holloway, A.E. Childress, K.E. Dennett, T.Y. Cath, Forward osmosis for concentration of anaerobic digester centrate, Water Res., 41 (2007) 4005–4014.

[6] M. Eyvaz, T. Aslan, S. Arslan, E. Yuksel, I. Koyuncu, Recent developments in forward osmosis membrane bioreactors: a comprehensive review, Desal. Wat. Treat., 57 (2016) 28610–28645.

[7] G. Han, S. Zhang, X. Li, T.S. Chung, Progress in pressure retarded osmosis (PRO) membranes for osmotic power generation, Prog. Polym. Sci., 51 (2015) 1–27.

[8] V.S. Anna, L.D.F. Marczak, I.C. Tessaro, Membrane concentration of liquid foods by forward osmosis: process and quality view, J. Food Eng., 111 (2012) 483–489.

[9] S. Zhao, L. Zou, C.Y. Tang, D. Mulcahy, Recent developments in forward osmosis: opportunities and challenges, J. Membr. Sci., 396 (2012) 1–21.

[10] B. Mi, M. Elimelech, Chemical and physical aspects of organic fouling of forward osmosis membranes, J. Membr. Sci., 320 (2008) 292–302.

[11] D. Li, Y. Yan, H. Wang, Recent advances in polymer and polymer composite membranes for reverse and forward osmosis processes, Prog. Polym. Sci., 61 (2016) 104–155.

[12] J.H. Jhaveri, Z.V.P. Murthy, A comprehensive review on anti-fouling nano-composite membranes for pressure driven membrane separation processes, Desalination, 379 (2016) 137–154.

[13] J. Wei, C. Qiu, C.Y. Tang, R. Wang, A.G. Fane, Synthesis and characterization of flat-sheet thin film composite forward osmosis membranes, J. Membr. Sci., 372 (2011) 292–302.

[14] J. Ren, B. O'Grady, G. deJesus, J.R. McCutcheon, Sulfonated polysulfone supported high performance thin film composite membranes for forward osmosis, Polymer, 103 (2016) 486–497.

[15] M.J. Park, S. Phuntsho, T. He, G.M. Nisola, L.D. Tijing, X.M. Li, G. Chen, W.J. Chung, H.K. Shon, Graphene oxide incorporated polysulfone substrate for the fabrication of flat-sheet thin-film composite forward osmosis membranes, J. Membr. Sci., 493 (2015) 496–507.

[16] M. Son, V. Novotny, H. Choi, Thin-film nanocomposite membrane with vertically embedded carbon nanotube for forward osmosis, Desal. Wat. Treat., 57 (2016) 26670–26679.

[17] N. Ma, J. Wei, R. Liao, C.Y. Tang, Zeolite-polyamide thin film nanocomposite membranes: towards enhanced performance for forward osmosis, J. Membr. Sci., 405–406 (2012) 149–157.

[18] M. Amini, A. Rahimpour, M. Jahanshahi, Forward osmosis application of modified TiO$_2$-polyamide thin film nanocomposite membranes, Desal. Wat. Treat., 57 (2016) 14013–14023.

[19] M. Amini, M. Jahanshahi, A. Rahimpour, Synthesis of novel thin film nanocomposite (TFN) forward osmosis membranes using functionalized multi-walled carbon nanotubes, J. Membr. Sci., 435 (2013) 233–241.

[20] L. Shen, S. Xiong, Y. Wang, Graphene oxide incorporated thin-film composite membranes for forward osmosis applications, Chem. Eng. Sci., 143 (2016) 194–205.

[21] F. Shao, L. Dong, H. Dong, Q. Zhang, M. Zhao, L. Yu, B. Pang, Y. Chen, Graphene oxide modified polyamide reverse osmosis membranes with enhanced chlorine resistance, J. Membr. Sci., 525 (2017) 9–17.

[22] Y. Heo, H. Im, J. Kim, The effect of sulfonated graphene oxide on sulfonated poly (Ether Ether Ketone) membrane for direct methanol fuel cells, J. Membr. Sci., 425–426 (2013) 11–22.

[23] S. Ayyaru, Y.H. Ahn, Application of sulfonic acid group functionalized graphene oxide to improve hydrophilicity, permeability, and antifouling of PVDF nanocomposite ultrafiltration membranes, J. Membr. Sci., 525 (2017) 210–219.

[24] G. Chen, H. Sun, S. Hou, Electrochemistry and electrocatalysis of myoglobin immobilized in sulfonated graphene oxide and Nafion films, Anal. Biochem., 502 (2016) 43–49.

[25] Y.H. Cho, J. Han, S. Han, M.D. Guiver, H.B. Park, Polyamide thin-film composite membranes based on carboxylated polysulfone microporous support membranes for forward osmosis, J. Membr. Sci., 445 (2013) 220–227.

[26] Y. Zhao, X. Wang, Y. Ren, D. Pei, Mesh-embedded polysulfone/sulfonated polysulfone supported thin film composite membranes for forward osmosis, ACS Appl. Mater. Interface 10 (2018) 2918–2928.

[27] Y. Zhao, Y. Ren, X. Wang, P. Xiao, E. Tian, J. Li, An initial study of EDTA complex based draw solutes in forward osmosis process, Desalination, 378 (2016) 28–36.

[28] A. Tiraferri, N.Y. Yip, A.P. Straub, S.R.V. Castrillon, M. Elimelech, A method for the simultaneous determination of transport and structural parameters of forward osmosis membranes, J. Membr. Sci., 444 (2013) 523–538.

[29] T. Kuila, S. Bose, A.K. Mishra, P. Khanra, N. Kim, J. Lee, Chemical functionalization of graphene and its applications, Prog. Mater. Sci., 57 (2012) 1061–1105.

[30] T.P.N. Nguyen, B.M. Jun, J.H. Lee, Y.N. Kwon, Comparison of integrally asymmetric and thin film composite structures for a desirable fashion of forward osmosis membranes, J. Membr. Sci., 495 (2015) 457–470.

[31] K.A. Mahmoud, B. Mansoor, A. Mansour, M. Khraisheh, Functional graphene nanosheets: the next generation membranes for water desalination, Desalination, 356 (2015) 208–225.

[32] I.C. Kim, S.H. Ahn, Y.S. Jin, B.S. Kim, Y.I. Park, J. Jegal, S.H. Lee, Y.N. Kwon, H.W. Rhee, Preparation of newly synthesized forward osmosis membrane, Desal. Wat. Treat., 51 (2013) 5191–5195.

[33] J. Ma, J. Liu, W. Zhu, W. Qin, Solubility study on the surfactants functionalized reduced graphene oxide, Colloids Surf., A, 538 (2018) 79–85.

[34] J. Deruiter, Carboxylic Acid Structure and Chemistry: Part 1, Principles of Drug Action 1, Spring, 2005, pp. 1–11.

[35] H. Chae, J. Lee, C.H. Lee, I.C. Kim, P.K. Park, Graphene oxide-embedded thin-film composite reverse osmosis membrane with high flux, anti-biofouling, and chlorine resistance, J. Membr. Sci., 483 (2015) 128–135.

[36] X. Wang, X. Wang, P. Xiao, J. Li, E. Tian, Y. Zhao, Y. Ren, High water permeable free-standing cellulose triacetate/graphene oxide membrane with enhanced anti-biofouling and mechanical properties for forward osmosis, Colloids Surf., A, 508 (2016) 327–335.

[37] D. Xiao, C.Y. Tang, J. Zhang, W.C.L. Lay, R. Wang, A.G. Fane, Modeling salt accumulation in osmotic membrane bioreactors: implications for FO membrane selection and system operation, J. Membr. Sci., 366 (2011) 314–324.

[38] S.E. Kwan, E. Bar-Zeev, M. Elimelech, Biofouling in forward osmosis and reverse osmosis: measurements and mechanisms, J. Membr. Sci., 493 (2015) 703–708.

[39] S.S. Bucs, R.V. Linares, J.S. Vrouwenvelder, C. Picioreanu, Biofouling in forward osmosis systems: an experimental and numerical study, Water Res., 106 (2016) 86–97.

[40] A. Bogler, S. Lin, E. Bar-Zeev, Biofouling of membrane distillation, forward osmosis and pressure retarded osmosis: principles, impacts and future directions, J. Membr. Sci., 542 (2017) 378–398.

[41] A. Tiraferri, Y. Kang, E.P. Giannelis, M. Elimelech, Superhydrophilic thin-film composite forward osmosis membranes for organic fouling control: fouling behavior and antifouling mechanisms, Environ. Sci. Technol., 46 (2012) 11135–11144.

[42] D.G. Kim, H. Kang, S. Han, J. Lee, The increase of antifouling properties of ultrafiltration membrane coated by star-shaped polymers, J. Mater. Chem., 22 (2012) 8654–8661.